

Failure Analysis and Mechanical Characterization of 3D Printed ABS With Respect to Layer Thickness and Orientation

Behzad Rankouhi · Sina Javadpour · Fereidoon Delfanian · Todd Letcher

Submitted: 3 April 2016 / Published online: 3 May 2016
© ASM International 2016

Abstract In contrast to conventional subtractive manufacturing methods which involve removing material to reach the desired shape, additive manufacturing is the technology of making objects directly from a computer-aided design model by adding a layer of material at a time. In this study, a comprehensive effort was undertaken to represent the strength of a 3D printed object as a function of layer thickness by investigating the correlation between the mechanical properties of parts manufactured out of acrylonitrile butadiene styrene (ABS) using fused deposition modeling and layer thickness and orientation. Furthermore, a case study on a typical support frame is done to generalize the findings of the extensive experimental work done on tensile samples. Finally, fractography was performed on tensile samples via a scanning digital microscope to determine the effects of layer thickness on failure modes. Statistical analyses proved that layer thickness and raster orientation have significant effect on the mechanical properties. Tensile test results showed that samples printed with 0.2 mm layer thickness exhibit higher elastic modulus and ultimate strength compared with 0.4 mm layer thickness. These results have direct influence on decision making and future use of 3D printing and functional load bearing parts.

Keywords 3D-printing · Layer thickness · Failure analysis · Mechanical properties · ANOVA Tukey HSD

Introduction

Complex geometries have always been out of reach for designers and manufacturers until the advent of additive manufacturing (AM) in the 1980s. ASTM defines the process as the “process of joining materials to make objects from three-dimensional (3D) model data, usually layer upon layer, as opposed to subtractive manufacturing methodologies” [1]. AM is a very broad term which encompasses numerous methods such as binder jetting, direct metal laser sintering (DMLS[®]), fused deposition modeling (FDM), powder bed fusion, and stereolithography. The FDM technique is of particular interest due to its association with desktop 3D printers. The term 3D printing is often used synonymously with AM, but is more commonly associated with machines that are low end in price and/or overall capability [1] and it usually refers to polymers and non-metal materials. The emergence of this term in the early 2010s made the technology popular among engineers and mainstream in public. This popularity has led the technology to become one of the fastest growing technologies in the world [2].

The FDM process works as follows: a thermoplastic polymer in form of a filament is extruded through a moveable nozzle head where it is deposited as a thread of molten material (raster) on a substrate (bed), usually made of glass or aluminum. Threads then solidify to form a layer of material. Additional layers are then deposited on top of each other to form a 3D object. So far, FDM has been mainly used in demonstrations, presentation models, visual aids, and education which include almost 25% of customer use in the AM industry [3]. Efforts have been undertaken during the past few years to prepare FDM to enter the realm of functional components which accounts for 29% of customer use (Fig. 1) [3]. The foremost obstacle facing to

B. Rankouhi · S. Javadpour · F. Delfanian · T. Letcher (✉)
Mechanical Engineering, South Dakota State University, Dept
PO Box 2219, Brookings, SD 57007-2201, USA
e-mail: todd.letcher@sdstate.edu

B. Rankouhi
e-mail: behzad.rankouhi@sdstate.edu

this transition is the limited knowledge regarding the mechanical properties of printed parts. When it comes to functionality, structural integrity is of the highest importance. In order to achieve a desirable strength, the manufacturing process and, in turn, the final product properties need to be standardized. Lack of standards for FDM manufacturing and testing has led to incongruent conclusions of test results and print settings. For example, tensile properties of acrylonitrile butadiene styrene (ABS) material manufactured using FDM have been reported to be between 11 and 40 MPa [4–8]. This divergence can be partially explained by taking the anisotropic nature of printed parts into account [8]. Another impediment is the large number of influential variables in the FDM process (Fig. 2). Controlling all of these parameters is a perplexing task especially when there are no standards available for reference.

Some work has been done to optimize some of these parameters for strength and design. Rodriguez et al. [9] utilized an integrated process-materials-design methodology to optimize the mechanical properties of parts fabricated using FDM for raster orientation aimed at moving FDM into volume production and functional components domain. Kara et al. [10] took a different approach in addressing the same problem. They used a surrogate-based optimization technique to improve load-carrying capacities of 3D printed parts by finding the optimum build orientation. Khan et al. [11] attempted to optimize different printing parameters, such as layer thickness, raster angle, and air gap size, to achieve maximum flexibility of the final part. Furthermore, effects of raster orientation on mechanical properties of parts fabricated using FDM have been extensively studied [2, 4, 7, 8]. All agree that the strongest printing orientation is always along the pull direction.

Fig. 1 Organizations’ use of industrial AM systems for a range of applications [3]

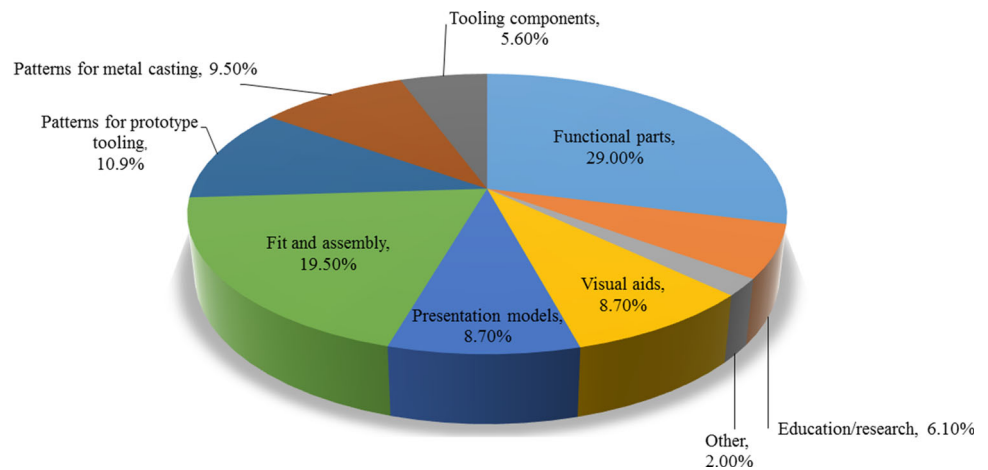
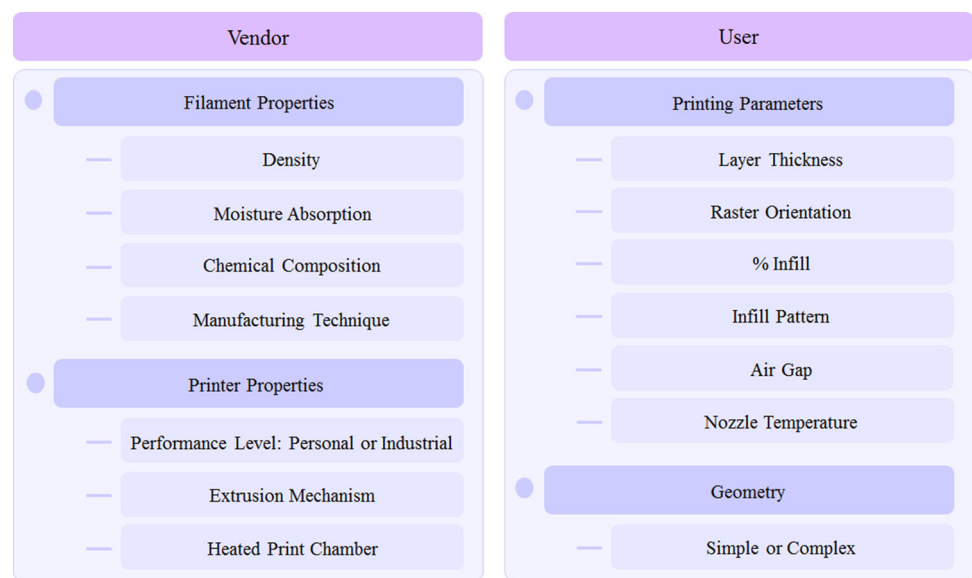


Fig. 2 Influential parameters on mechanical properties of parts fabricated using FDM



A more controversial parameter is the layer thickness. Khan et al. [11] concluded that the optimal set of parameters for maximum performance of their model always include the smallest layer thickness (0.178 mm), while Sood et al. [12] stated that the tensile strength of their samples first decreased and then increased as the layer thickness increased. They associated the partial increase in strength with stronger diffusion between adjacent rasters due to high-temperature gradients. They also hypothesized that the decrease in strength is due to the large number of heating and cooling cycles and the consequent residual stresses that follow. On the other hand, Tymark et al. [4] inferred that samples with the largest layer thickness showed higher elastic modulus and samples with the lowest layer thickness had the highest tensile strength. Ahn et al. [8] deduced a low level of significance for effects of layer thickness on tensile strength of ABS specimens. Moreover, Anitha et al. [13] reported 51.57% effectiveness at 99% level of significance for effects of layer thickness on surface roughness of components produced using FDM. Effects of layer thickness have been studied in other forms of 3D printing processes as well [14]. None of the aforementioned studies have thoroughly investigated the effects of layer thickness. The inconsistency in reported results is another indication that effects of printing parameters on

mechanical properties of parts still need to be studied, particularly in regard to layer thickness.

The use of FDM machines for manufacturing functional parts is rapidly growing, especially in fields of biomedical and robotic engineering [15–20] and is transitioning from a do-it-yourself hobbyist machine into a more robust and reliable manufacturing system. To help expedite this transition, a comprehensive knowledge of the influential parameters on mechanical properties of manufactured parts is required. The work presented in this paper attempts to address the debatable layer thickness effects on the mechanical properties of 3D printed ABS samples using FDM through a set of extensive tensile tests followed by statistical analysis of the results. It is an extension of a preliminary study by Letcher et al. [2]. In addition, a failure analysis is presented via microscopic inspection of fracture areas and air-gap measurements. The practicality of results was further demonstrated by testing a typical A-Frame as a case example. The proposed findings can help designers and manufacturers to better understand the effects of print parameters on their components and make engineering decisions by evaluating time, material usage, and strength of the final product.

Experimental Setup

The goal of this study was to investigate the correlation between layer thickness and mechanical properties of additively manufactured parts using FDM. In order to do so, mechanical tensile tests were performed on samples made of ABS, one of the most common materials used for FDM process. ABS is a thermoplastic polymer, a material which becomes moldable at a relatively low glass transition temperature and solidifies upon cooling. Other prevalent thermoplastic polymers used in FDM process are PLA, PEEK, ULTEM, nylon, and polycarbonate (PC).

The first step in designing the experiment was choosing the geometry of the specimens. There are no specific standard test methods available for parts fabricated using FDM. ASTM D638 [21] is the best available choice for preparing samples; however, there have been reports of premature failure of 3D printed parts during testing due to

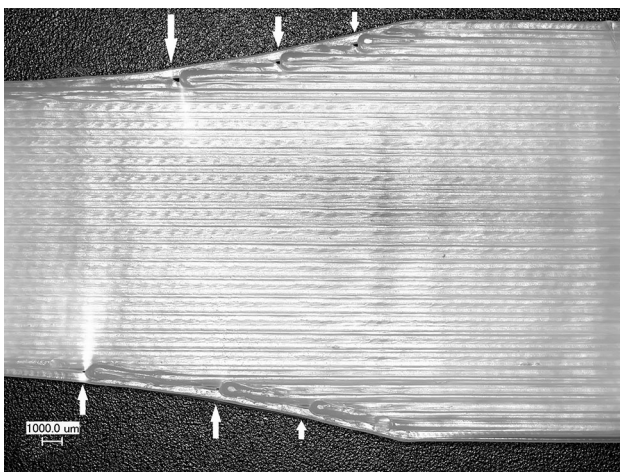
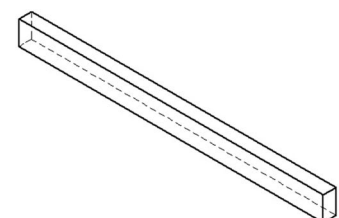


Fig. 3 Stress concentration due to raster discretization at fillet radius of a 0°, ASTM D638 sample

Fig. 4 Tensile test specimen with its dimensions in mm



accumulated stress concentration at fillet areas [2, 5, 6, 8]. This stress concentration is mainly caused by raster termination near the fillet radius as shown by arrows in Fig. 3. Increasing the number of layers can help alleviate the effects of this stress concentration by gradually filling the gaps as each layer deposits on top of the other. But thin samples, specimens that are made of a single or only a few layers, will still be affected by the discretization of rasters at fillets. To alleviate this issue, ASTM D3039 [22] guidelines were used to prepare the tensile testing samples (Fig. 4). According to this standard, “design of mechanical test coupons remains to a large extent an art rather than a science, with no industry consensus on how to approach the engineering of the gripping interface.” This statement can be extended to parts manufactured by FDM process as well and is an indication of the anisotropic effects of these parts on their mechanical properties. Samples were printed using an entry level 3D printer Makerbot Replicator 2x. Custom print profiles were created to allow the printer to build samples with a single raster orientation throughout. Figure 5 depicts the orientations used with respect to pulling direction. To minimize the effects of uncontrolled

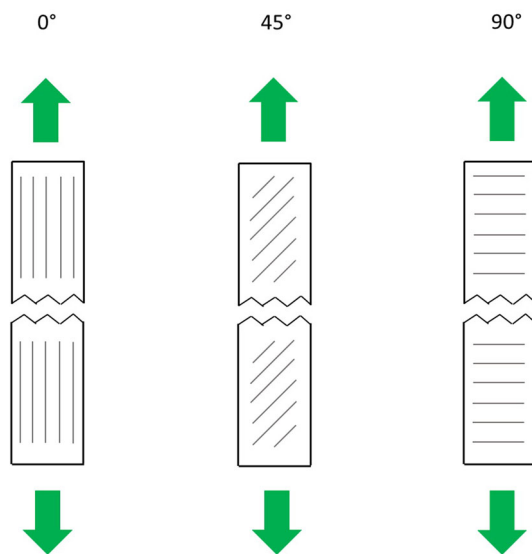


Fig. 5 Printed raster orientations with respect to pulling direction

parameters on the mechanical properties of printed parts, each sample was printed individually at the exact same position on the bed. A single perimeter was used for all samples to reduce its strengthening effects as reported by Croccolo et al. [6]. All samples were printed at 100% density. Using maximum infill can cause raster overlap or negative air-gap size, which, in turn, influences on the strength of the material [2]. The effects of air-gap size will be investigated in the results and discussion section of this paper. In this study, default settings were used on Makerware® software and raster overlapping was not a controlled variable throughout testing. All specimens were printed using the same generic brand of ABS filament.

For comparison purposes, controlled printing parameters are tabulated in Table 1. Two nominal layer thicknesses

Table 2 Tensile test specimens in details

0.2 mm Layer thickness		0.4 mm Layer thickness	
Number of layers	Nominal thickness	Number of layers	Nominal thickness
1	0.2	1	0.4
2	0.4	2	0.8
3	0.6	3	1.2
4	0.8	4	1.6
5	1.0	5	2
6	1.2	6	2.4
7	1.4	7	2.8
8	1.6	8	3.2
9	1.8	9	3.6
10	2	10	4
11	2.2	11	4.4
12	2.4	12	4.8
15	3	15	6
20	4	18	7.2
25	5		
30	6		
35	7		
Population per orientation	68	Population per orientation	56

Table 1 Controlled printing parameters

Parameter	0.2 mm Layer thickness		0.4 mm Layer thickness	
	Layers 1 to 3	Layers 4 to 35	Layers 1 and 2	Layers 3 to 18
Infill density (%)	100	100	100	100
Feed rate (mm/s)	30	90	30	90
Extruder temperature (°C)	230	230	230	230
Bed temperature (°C)	70	110	70	110
Number of shells	1	1	1	1

were considered in this study, 0.2 and 0.4 mm. The thinnest samples have only one layer with nominal thickness of 0.2 and 0.4 mm. The thickest samples have 35 layers and 7 mm nominal thickness and 18 layers and nominal thickness of 7.2 mm for 0.2 and 0.4 mm treatments, respectively. Actual thickness and width were individually measured for each specimen using a caliper and minimum dimensions were used for performing calculations according to testing standards. A total of 372 samples were tested in this study. Four samples were tested for each layer number. Table 2 shows details of samples used as tensile test specimens in this study.

Tests were conducted using an MTS Insight 5 system with a 5 kN load cell. Built-in LVDTs measured the displacement between the grips. To calculate the strain, the distance between the grips was considered as initial gage length. Tests were carried out according to ASTM D638 [21] at room temperature. The MTS pneumatic grips were displaced at the rate of 5 mm/min with data collected at 100 Hz. There are two important outputs: load and displacement. To ensure that failure occurred in the gage section and that high grip pressure did not apply stress concentration on the specimens, grip pressure was

manually controlled with the low at 173 KPa and the high at 275 KPa. To better understand the effects of layer thickness on failure modes of specimens, microscopic inspection was performed utilizing a Keyence VHX-600 digital microscope. Furthermore, air-gap to material ratio calculations on fracture surface areas of samples with 0.2

Table 3 Details of the A-frame samples for tensile test

Layer thickness (mm)	
0.2	0.4
Orientation	Orientation
Default	Default
0°	0°
45°	45°
90°	90°

Sample size $n = 3$

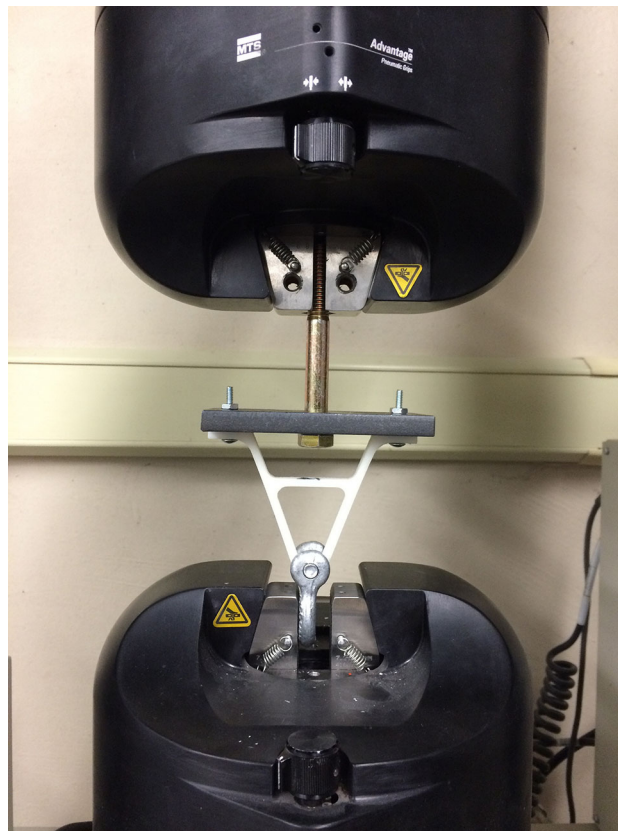


Fig. 7 Test setup for determining the strength of an A-frame as a functional load bearing part

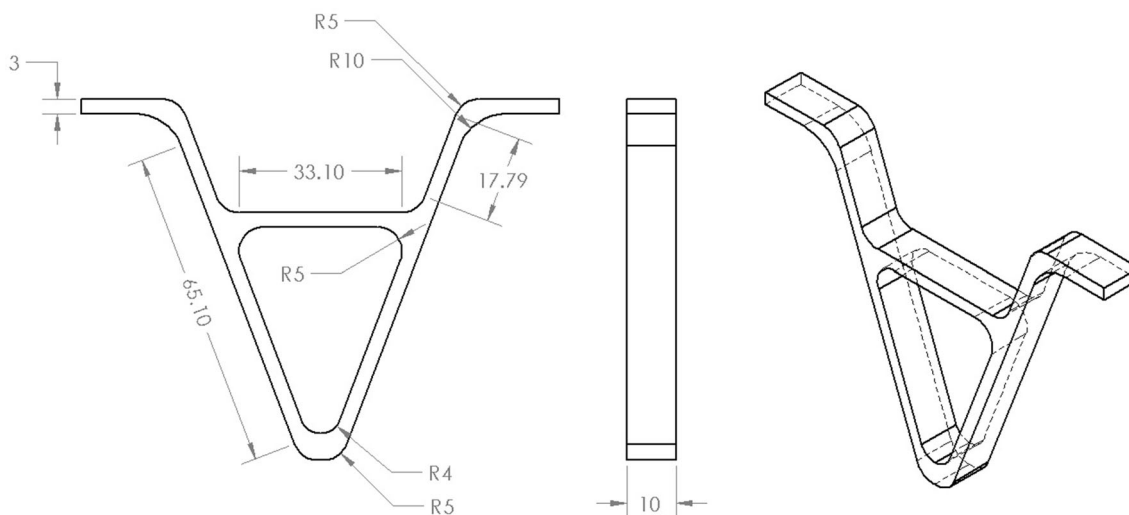


Fig. 6 A-frame geometry and its main dimensions in mm

Table 4 Tensile test results for specimens with 0.2 mm layer thickness

Number of Layers	0° Raster Orientation				45° Raster Orientation				90° Raster Orientation			
	Ultimate Strength (MPa)		Elastic Modulus (MPa)		Ultimate Strength (MPa)		Elastic Modulus (MPa)		Ultimate Strength (MPa)		Elastic Modulus (MPa)	
	Mean	σ	Mean	σ	Mean	σ	Mean	σ	Mean	σ	Mean	σ
1	32.2	6.4	1818.4	289.1	9.2	3.0	1219.5	177.0	3.9	1.0	550.3	151.5
2	30.3	1.4	1754.3	57.0	21.4	1.6	1561.5	97.6	12.1	1.1	1264.2	36.9
3	33.7	1.5	1812.9	47.7	23.8	4.2	1665.5	126.0	22.0	2.6	1519.5	20.0
4	32.9	1.7	1800.0	47.1	28.9	1.4	1755.2	88.2	26.4	0.4	1606.6	21.4
5	32.2	1.6	1750.6	57.1	30.0	1.3	1822.4	95.1	28.0	0.4	1682.1	36.3
6	35.4	1.6	1915.9	97.0	30.6	1.6	1801.1	106.4	28.2	0.7	2111.6	65.3
7	35.7	1.2	2107.3	79.2	30.8	0.9	1796.5	75.0	28.7	1.0	2125.3	92.2
8	35.5	1.7	2127.9	34.7	31.3	1.8	1979.9	64.7	30.3	0.3	2153.9	90.3
9	36.7	0.5	2055.7	105.3	32.2	1.4	2021.1	43.7	30.5	0.5	2196.1	50.0
10	37.2	0.2	2148.2	140.2	32.8	0.4	2092.0	73.0	31.3	0.1	2045.6	74.3
11	37.7	0.3	2093.9	99.0	34.3	0.6	2131.9	42.0	31.7	0.3	2103.0	44.6
12	37.5	0.6	2106.2	145.5	35.5	0.1	2224.8	72.7	31.3	0.1	2133.8	68.1
15	34.6	0.7	2123.9	50.6	34.1	0.2	2195.4	47.7	31.8	0.5	2193.7	45.8
20	38.7	0.8	2175.9	53.4	35.8	0.7	2193.1	92.2	31.6	0.4	2172.1	61.0
25	38.0	1.3	2160.0	83.1	36.1	0.3	2230.5	87.9	31.7	1.0	2140.9	61.5
30	38.7	0.6	2054.3	127.3	35.7	2.0	2128.0	67.8	32.5	0.4	2072.9	59.3
35	39.4	0.3	2221.3	90.6	35.8	0.1	2157.2	27.6	31.6	0.6	2076.1	104.2

Table 5 Tensile test results for specimens with 0.4 mm layer thickness

Number of layers	0° Raster orientation				45° Raster orientation				90° Raster orientation			
	Ultimate strength (MPa)		Elastic modulus (MPa)		Ultimate strength (MPa)		Elastic modulus (MPa)		Ultimate strength (MPa)		Elastic modulus (MPa)	
	Mean	σ	Mean	σ	Mean	σ	Mean	σ	Mean	σ	Mean	σ
1	26.0	3.1	1604.1	91.9	14.5	2.3	1232.6	108.2	17.1	1.6	1397.4	123.5
2	29.0	1.6	1717.3	57.2	18.2	1.1	1325.0	48.1	24.1	0.6	1651.5	35.1
3	29.0	1.6	1741.2	37.0	23.1	0.4	1492.4	30.7	17.9	1.4	1317.6	47.0
4	29.2	2.6	1725.7	27.6	25.1	0.4	1545.1	10.9	27.8	0.5	1782.2	48.7
5	29.5	1.5	1757.5	27.8	27.6	0.4	1627.0	45.5	27.7	0.6	1766.1	14.4
6	29.8	1.2	1760.8	7.1	30.5	0.5	1775.4	50.0	28.0	0.2	1790.4	17.6
7	29.5	1.6	1772.6	12.7	29.5	0.2	1729.5	8.3	28.0	0.1	1764.7	23.8
8	30.3	0.7	1786.6	26.5	29.5	0.6	1708.8	33.8	26.9	0.4	1743.0	32.0
9	30.6	0.2	1803.6	5.6	29.4	0.7	1697.4	19.3	26.3	1.5	1767.9	49.6
10	32.0	1.4	1808.6	21.2	28.8	0.1	1721.3	25.4	27.5	0.2	1814.7	6.3
11	32.5	0.2	1749.5	27.1	28.3	1.4	1637.3	61.5	28.8	0.2	1785.4	43.4
12	32.4	0.9	1755.9	23.4	29.7	0.4	1750.4	49.3	28.1	0.3	1799.0	13.4
15	30.9	1.0	1678.7	57.9	29.1	1.3	1658.1	71.3	26.5	1.3	1787.2	30.3
18	33.0	0.6	1720.8	32.6	30.0	0.9	1652.7	30.0	28.4	0.1	1760.1	14.6

and 0.4 mm of layer thicknesses were done using a built-in function of the system's image processing software.

Finally, to demonstrate the approach in a more practical way, tensile tests were performed on an A-frame

manufactured out of the same generic brand of ABS filament and under the same printing conditions (Table 1). Samples were printed in 0.2 and 0.4 mm layer thicknesses with different orientations using customized printing profiles of

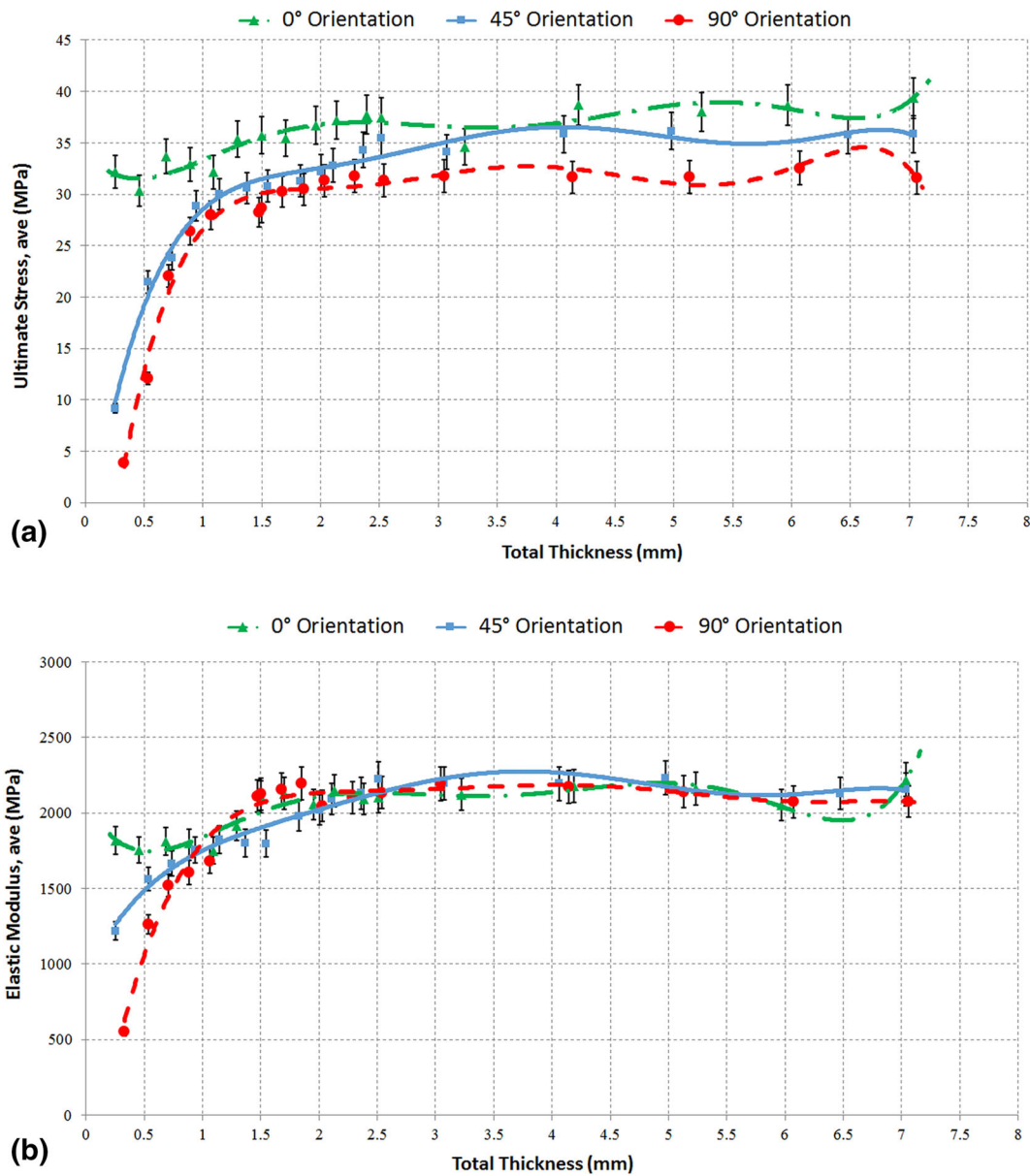


Fig. 8 Mechanical strength of specimens with 0.2 mm layer thickness with respect to the total thickness: **(a)** mean of ultimate strength vs. total thickness of samples. **(b)** mean of elastic modulus vs. total thickness of samples

Makerware® software. Details on test samples for this case example are tabulated in Table 3. It should be noted that default orientation is a combination of 0°, 45°, and 90° orientations determined by Makerware® software. Figure 6 depicts the geometry of the proposed frame with its main dimensions. Testing was done utilizing the same MTS Insight 5 testing system with 5 mm/min displacement rate. In actual practice, functional parts endure two types of loading: static and dynamic. The A-frame is designed to serve as a functional static load-bearing structural component. A customized fixture was used in order to simulate a hypothetical working condition of the frame during testing. The test setup is shown in Fig. 7.

Results and Discussion

Tensile Test Results

An extensive experimental campaign was designed to study the effects of layer thickness on ultimate strength and elastic modulus of printed specimens at a range of layer thicknesses and raster orientations. Mean and standard deviation of test results are tabulated in Tables 4 and 5. To better understand the correlation between different thicknesses and orientations, graphical representations of the results are provided in Figs. 8, 9, 10 and 11. A first look at

the results reveals that 0° raster orientation showed mostly the highest values for ultimate strength and elastic modulus for both 0.2 and 0.4 mm layer thicknesses, while 90° raster orientation resulted in the lowest values for ultimate strength and elastic modulus. For 45° raster orientation, these values mostly fell between those of 0° and 90° orientations. These results confirm previous work done in this area [4, 5, 8].

This difference can be explained by considering inter-raster fusion bonds and tensile strength of each individual raster, known as trans-raster strength. The inter-raster fusion failure had the least influence on mechanical

Fig. 10 Graphical comparison of ultimate strength for specimens printed at (a) 0° raster orientation (b) 45° raster orientation and (c) 90° raster orientation

strength of specimens in 0° raster orientation, since each raster was pulled along its longitudinal axis, causing trans-raster tensile failure. For specimens with 90° raster orientation, force was exerted perpendicular to raster longitudinal axis resulting in inter-raster fusion failure. In this case, layer adhesion along with the shell number in specimens with 90° raster orientation significantly affects the tensile strength, since the inter-raster fusion bonds between adjacent rasters withstood most of the applied load

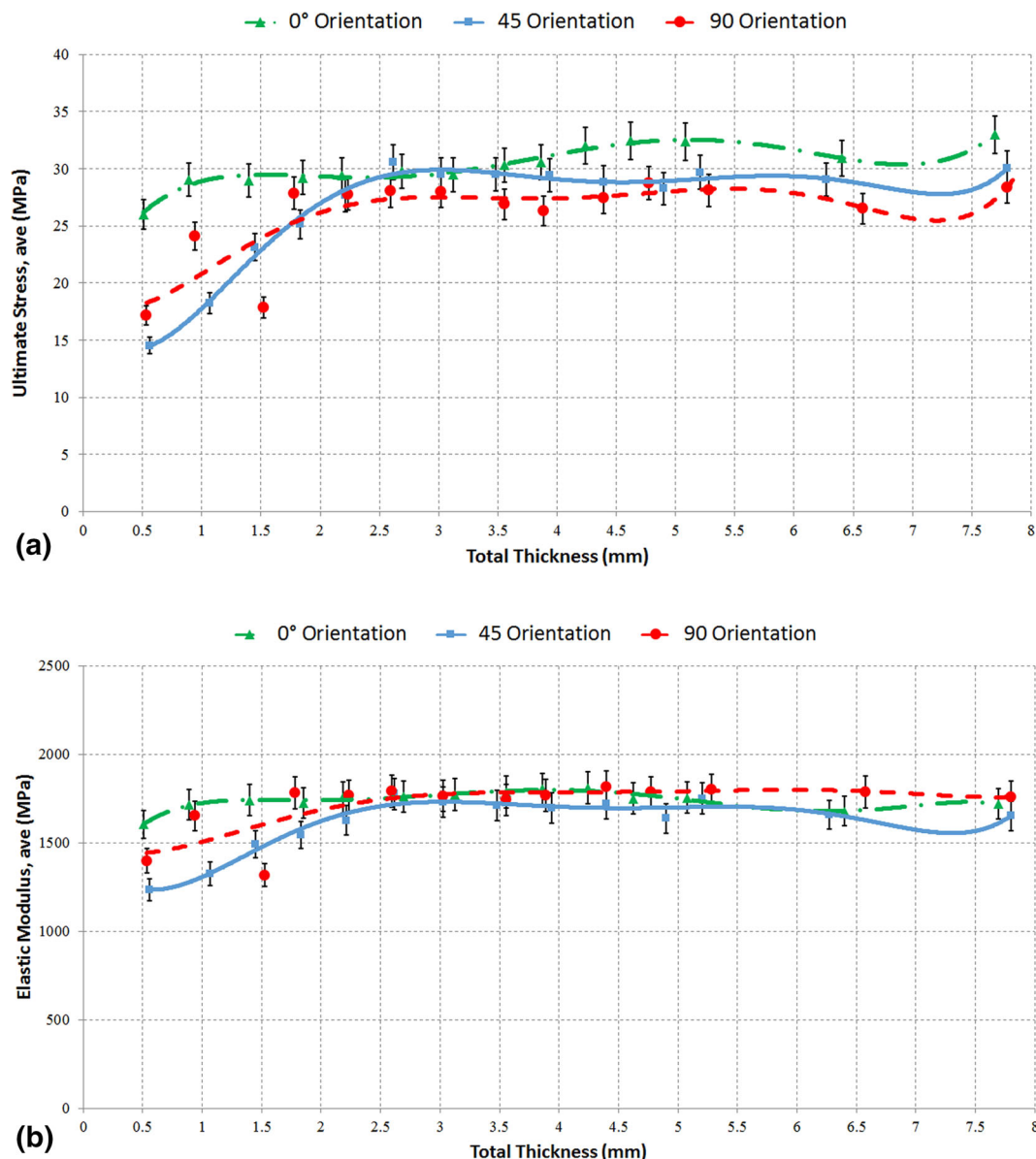
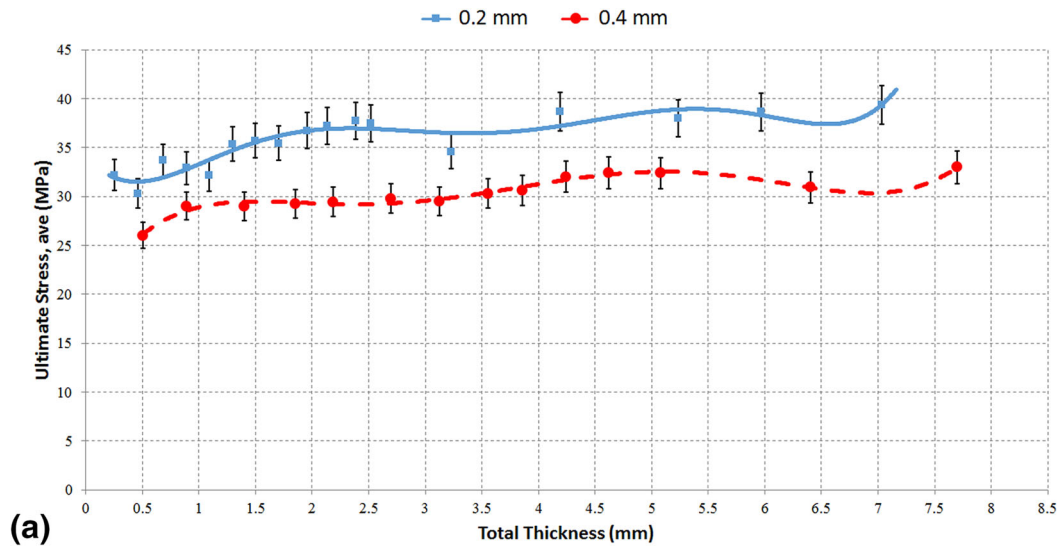
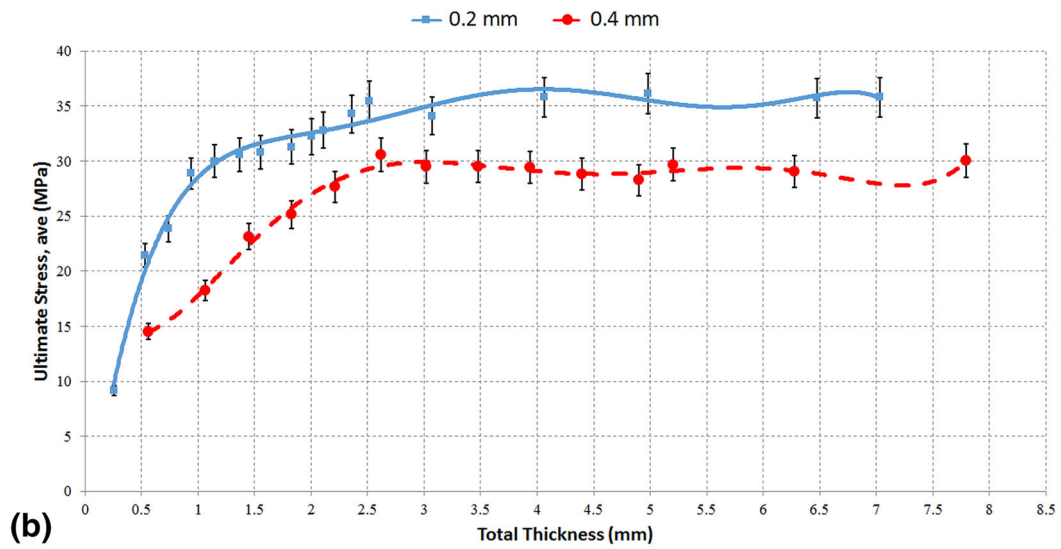


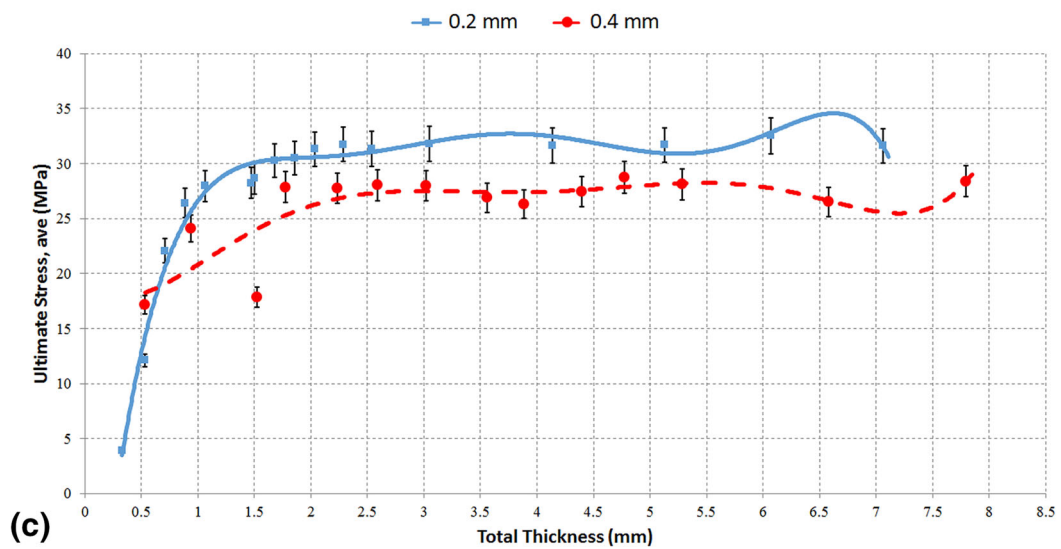
Fig. 9 Mechanical strength of specimens with 0.4 mm layer thickness with respect to the total thickness: (a) mean of ultimate strength vs. total thickness of samples. (b) mean of elastic modulus vs. total thickness of samples



(a)



(b)



(c)

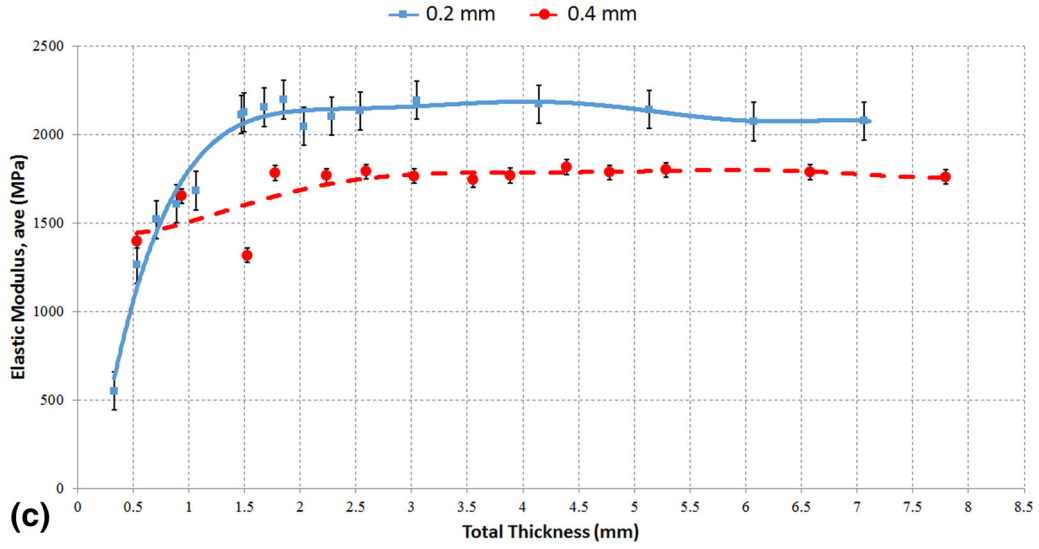
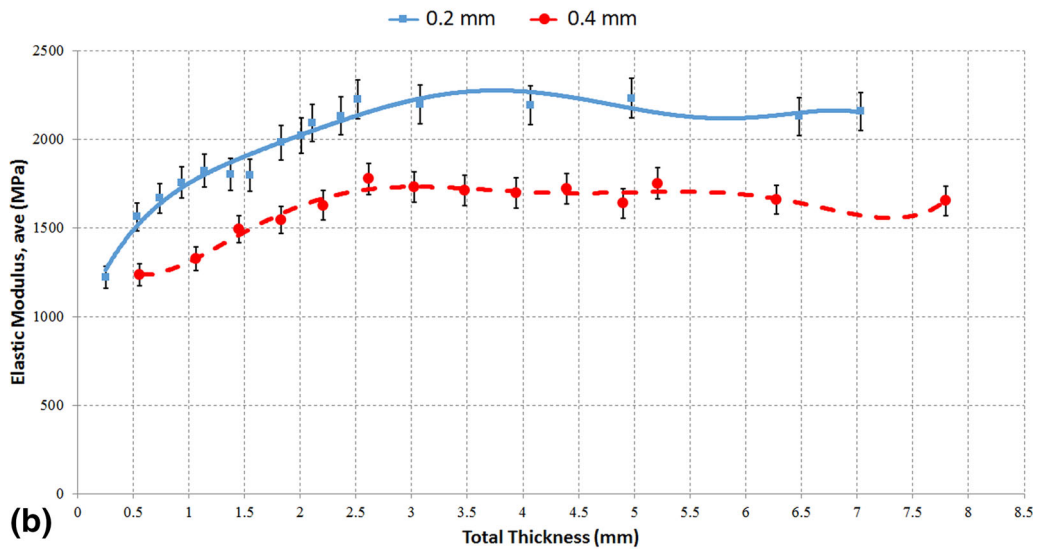
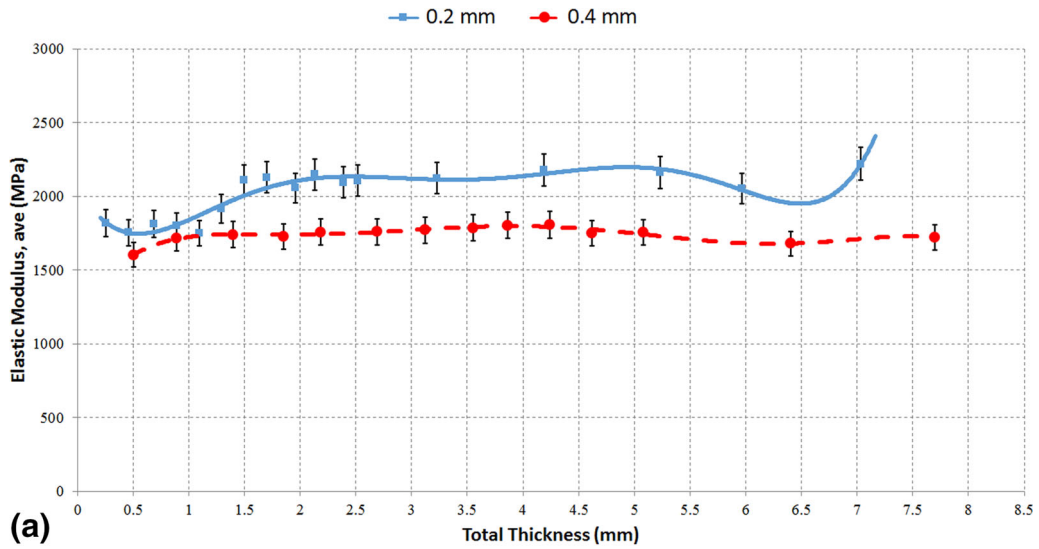


Fig. 11 Graphical comparison of elastic modulus for specimens printed at (a) 0° raster orientation (b) 45° raster orientation and (c) 90° raster orientation

[2]. Figures 8 and 9 provide graphical comparison for data presented in Tables 4 and 5. Comparison of 0.2 and 0.4 mm layer thicknesses showed that specimens with 0.4 mm layer thickness have less dependency on total thickness, whereas specimens with 0.2 mm layer thickness displayed significant dependency on total thickness, particularly up to 2 mm total thickness. At thicknesses lower than 2 mm, failure at a raster or a layer will lead to failure of the entire specimen, since there is simply not enough remaining material to withstand the applied stresses. On the other hand, at thicknesses higher than 2 mm, the amalgamation of layers compensates for the failure of single rasters or layers and, as a result, the curve for both ultimate strength and elastic modulus plateaued throughout the test.

Figures 10 and 11 compare the strength of specimens with respect to their layer thickness. It is evident that specimens with 0.2 mm layer thickness displayed higher values for ultimate strength and elastic modulus than specimens with 0.4 mm. For a more in-depth study of this comparison, a numerical calculation of air-gaps was carried out using Keyence VHX-600 digital microscope images. Built-in image processing software provided area calculation options based on brightness and contrast differences. Two rectangular specimens were printed with the exact same settings in 0.2 and 0.4 mm layer thicknesses and 0° raster orientation (Fig. 12). In order to preserve the structural integrity of specimens and to ensure that the geometry of gaps was not affected when being cut, an Instron Charpy impact tester was used to break specimens in half. Brittle fracture was ensured by cooling specimens to -29 °C. Air-gaps are generally categorized into three groups: (1) standard or zero, (2) positive, and (3) negative, as explained by

Li et al. [23]. As depicted in Fig. 12, rasters overlap each other when layers are deposited on top of one another, resulting in a negative air-gap. Based on the observation from these images, air-gaps appear periodically when the air-gap is negative. Results can be generalized for bigger cross-sectional areas. Calculations were completed on 7.6 mm² cross section area. As shown in Table 6, the air-gap to material ratio for 0.4 mm layer thickness specimen is 5.26%, while for 0.2 mm layer thickness it equals 0.3%. It can be concluded from the results that higher strength for specimens with 0.2 mm layer thickness is due to smaller air-gap to material ratio.

Statistical Analysis

Full factorial regression models were built and used for ANOVA analyses to investigate the effects of layer

Table 6 Air-gap to material ratio calculation for specimens printed at 0° raster orientation

Calculated property	0.2 mm layer thickness	0.4 mm layer thickness
Inspected area (mm ²)	7.6038	7.6038
Total air-gap area (mm ²)	0.0232	0.4
Number of air-gaps	218	182
Air-gap to material ratio (%)	0.3	5.26

Table 7 List of factors and their levels

Factor	Levels	Values
Layer thickness (LT)	2	0.2 mm, 0.4 mm
Orientation (O)	3	0°, 45°, 90°

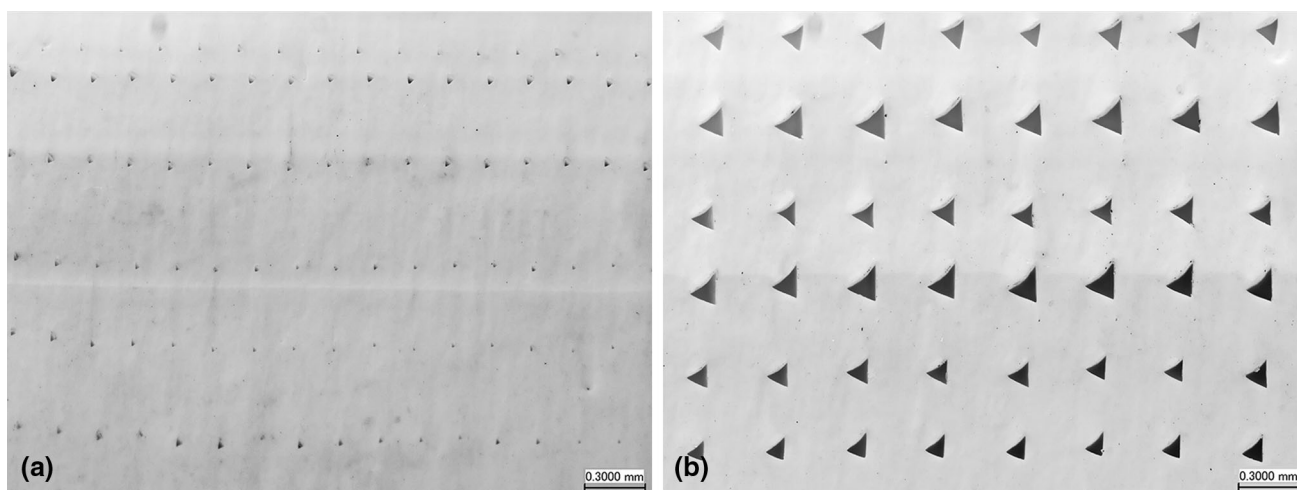
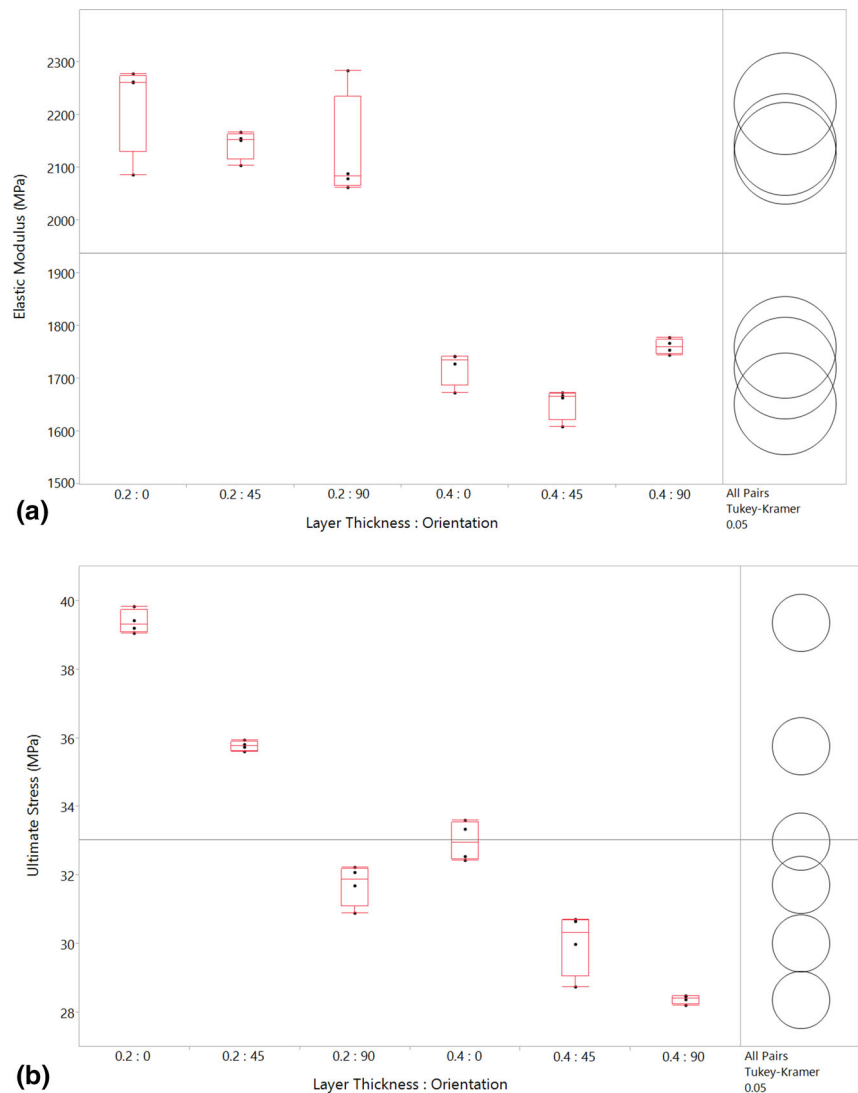


Fig. 12 Mesostructures of air-gaps for specimens with (a) 0.2 mm and (b) 0.4 mm layer thickness

Table 8 ANOVA analyses results

Source	DOF	Elastic modulus (MPa)				Ultimate strength (MPa)			
		SS	MS	<i>F</i>	<i>P</i> (> <i>F</i>)	SS	MS	<i>F</i>	<i>P</i> (> <i>F</i>)
LT (mm)	1	1,232,036.908	1,232,036.908	335.87	<0.0001	159.738	159.738	573.55	<0.0001
O (Degree)	2	21,649.359	10,824.679	2.95	0.0779	150.421	75.211	270.05	<0.0001
LT × O	2	21,906.664	10,953.332	2.99	0.0759	10.323	5.162	18.53	<0.0001
Error	18	66,027.912	3,668.217	–	–	5.013	0.279	–	–

Fig. 13 Tukey-Kramer results (a) elastic modulus vs. layer thickness (b) ultimate strength vs. layer thickness and orientation

thickness and raster orientation on mechanical properties of tensile test specimens, including elastic modulus and ultimate strength. Table 7 shows the factors in the models and their corresponding levels. Furthermore, the results from ANOVA analyses are provided in Table 8. Since the significance level (α) used in the analyses is set to 0.05, any factor or combination of factors having a *P* value of 0.05 or less is considered to have a significant effect on the

responses (mechanical properties), with the highest *F* value, having the most significance. Consequently, in the ANOVA analysis for elastic modulus, the only significant source was found to be the layer thickness. In the case of ultimate strength, however, layer thickness and orientation and also their combination were found to be significant, with the layer thickness having the most significant effect. The effect from the combination of factors was concluded

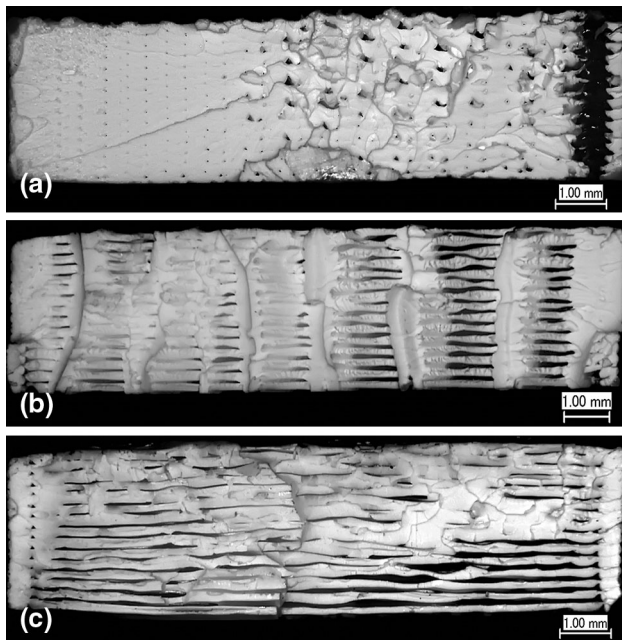


Fig. 14 Microscopic inspection of failure area of 0.2 mm layer thickness specimens at different orientations at 20x: (a) 0° raster orientation, (b) 45° raster orientation, (c) 90° raster orientation

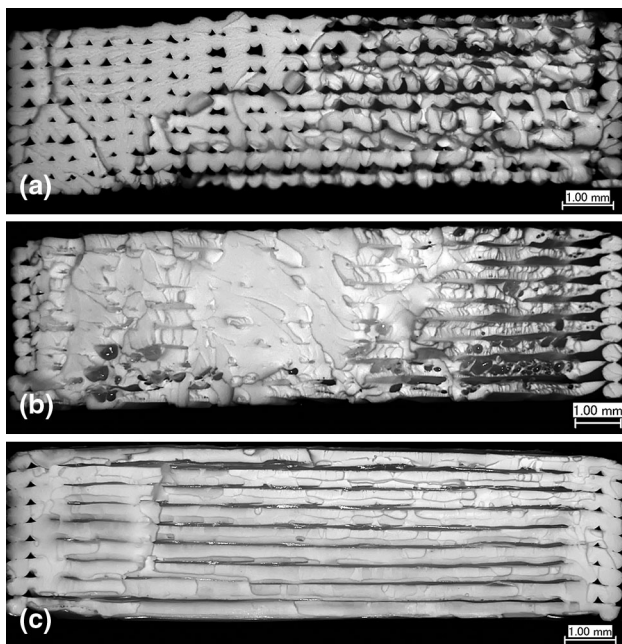


Fig. 15 Microscopic inspection of failure area of 0.4 mm layer thickness specimens at different orientations at 20x: (a) 0° raster orientation, (b) 45° raster orientation, (c) 90° raster orientation

to be marginal as its *F* value is relatively small when compared to those of the main effects of factors; hence, its significance originates from the significance of each individual factor.

Table 9 Tensile test results for the A-frame

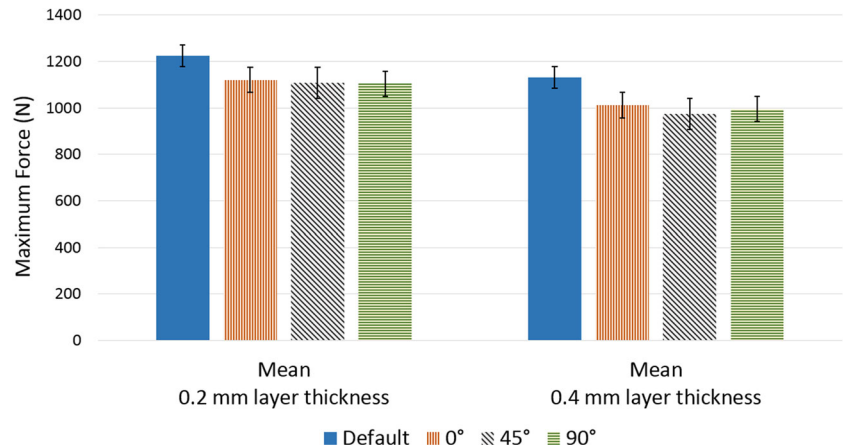
Raster orientation	Maximum force (N)			
	0.2 mm layer thickness		0.4 mm layer thickness	
	Mean	σ	Mean	σ
Default	1223.6	41.1	1130.9	36.2
0°	1120.9	33.3	1011.3	49.1
45°	1107.8	17.9	828.9	72.8
90°	1104.4	92.8	995.7	83.1

In addition to ANOVA analyses, all pairs Tukey-Kramer analyses were performed to determine how a change in significant factors would affect the mechanical properties and which specimens have the highest mechanical properties. Factors included in the models used for Tukey-Kramer analyses were chosen according to the results of the ANOVA table. Hence, for elastic modulus, results were compared based on the effect of the change in layer thickness only, while for ultimate strength, the effects of both layer thickness and orientation were considered. As shown in Fig. 13, the results of Tukey-Kramer tests from samples of 0.2 mm layer thickness have a significantly higher elastic modulus than those of 0.4 mm layer thickness. Ultimate strength has the highest value and is significantly different for samples with 0.2 mm layer thickness and 0° raster orientation. Samples with 0.2 mm layer thickness have significantly higher ultimate strengths compared to those with 0.4 mm layer thickness, except for 0.2 mm and 90° orientation which have slightly lower ultimate strengths than 0.4 mm and 0° raster orientation. For each layer thickness, ultimate strength is the highest for 0° raster orientation and keeps decreasing constantly when it is changed to 45° and then 90°. Samples with 0.4 mm layer thickness and 90° raster orientation have the lowest ultimate strengths, which are significantly lower than those of all other samples.

Microscopic Inspection

The fracture surface of specimens with 15 layers (at 0.2 mm layer thickness) and 9 layers (at 0.4 mm layer thickness) used as representatives of the entire population, are provided in Figs. 14 and 15, respectively. Comparison of fracture morphologies showed that failure modes are independent of layer thickness and change with respect to raster orientation. A comparison of Figs. 14a and 15a reveals the effect of larger air gaps on the fracture morphology of the specimens. It can be seen that larger air-gaps in the specimen with 0.4 mm layer thickness caused inter-raster fusion bonds to fail resulting in a more discretized surface area. Failure at specimens with 0° raster

Fig. 16 Comparison of the A-frame tensile test results



orientation is mainly associated with trans-raster failure which agrees with their resulting higher tensile strength. On the other hand, specimens with 90° raster orientation experienced a more brittle fracture since failure occurs mainly in inter-raster fusion bonds as shown in Figs. 14c and 15c. This conclusion also agrees with results obtained from tensile tests. Overall, there are two main failure modes for tested specimens: (1) inter-raster fusion bond failure, which is the main contributor to failure of samples printed in 45° and 90° raster orientations, regardless of their layer thickness; and (2) trans-raster failure, which is the main contributor to failure of specimens printed in 0° raster orientation, regardless of their layer thickness [24].

The A-Frame Test Results

An arbitrary “A”-shaped structural frame was designed and manufactured using the same printing settings mentioned in Table 1. Table 9 shows the mean and standard deviation for the maximum force at failure for each orientation and layer thickness. Due to the geometry of the part, instead of calculating stress, the maximum load at failure was considered for strength comparison. As expected from the tensile test results, samples with 0.2 mm layer thickness demonstrate higher mechanical strength compared to samples with 0.4 mm layer thickness. Effects of raster orientation are also as expected, with default orientation resulting in the highest value for force at failure, following by 0° orientation (Fig. 16). However, unlike the tensile test samples, the combination of layer thickness and raster orientation rather than layer thickness alone have a significant effect on the final strength of the material due to complex geometry of the frame.

Conclusion

The effects of layer thickness and raster orientation on mechanical properties of 3D printed specimens were

studied by running an extensive experimental campaign in order to address the controversy in the literature regarding the effects of layer thickness. Tensile test results along with statistical analyses of the data clearly suggest that specimens with 0.2 mm layer thickness are stronger than specimens with 0.4 mm layer thickness and that layer thickness and raster orientation both have a significant effect on the mechanical properties of material. This conclusion was also confirmed by testing an A-frame as a practical 3D printed part. The microscopic inspection of fracture area revealed that smaller air-gap to material ratio can be the main factor contributing to higher strength in these specimens.

As the FDM advances into a more practical and industrial method of manufacturing, in-depth understanding of less known printing parameters, such as layer thickness on the strength of the end user part, becomes paramount. The purpose of this study was to provide solid ground for designers and manufacturers on which they can make better engineering decisions by having all required information at hand.

Acknowledgments The authors would like to thank Joseph Robertson for his consultation on statistical analyses. The experiments presented in this study were performed in Material Evaluation and Testing Laboratory (METLAB) in the mechanical engineering department at South Dakota State University (SDSU). Financial support for this paper was provided by Advanced Manufacturing Process Technology Transition & Training Center (AMPTEC) under Contract Number 3S6674.

References

1. ASTM International, *Standard Terminology for Additive Manufacturing Technologies (Withdrawn 2015)—ASTM F2792-12a* (ASTM International, West Conshohocken, 2012)
2. T. Letcher, B. Rankouhi and S. Javadpour, Experimental study of mechanical properties of additively manufactured ABS plastic as a function of layer parameters, *ASME 2015 Int. Mech. Eng. Cong. and Exp.*, 2015, p. V02AT02A018-V02AT02A018.

3. “Wohler’s Report, 3D Printing and Additive Manufacturing State of the Industry, Annual Worldwide Progress Report”, 2014, Wohler’s Associates, 2015, p. 20.
4. B.M. Tymrak, M. Kreiger, J.M. Pearce, Mechanical properties of components fabricated with open-source 3-D printers under realistic environmental conditions. *Mater. Des.* **58**, 242–246 (2014)
5. A.R. Torrado, D.A. Roberson, Failure analysis and anisotropy evaluation of 3D-printed tensile test specimens of different geometries and print raster patterns. *J Fail. Anal. Preven.* **16**(1), 154–164 (2016)
6. D. Crococolo, M. De Agostinis, G. Olmi, Experimental characterization and analytical modelling of the mechanical behaviour of fused deposition processed parts made of ABS-M30. *Comp. Mat. Sci.* **79**, 506–518 (2013)
7. A. Bellini, S. Güçeri, Mechanical characterization of parts fabricated using fused deposition modeling. *Rapid Prototyp. J.* **9**(4), 252–264 (2003)
8. S. Ahn, M. Montero, D. Odell, S. Roundy, P.K. Wright, Anisotropic material properties of fused deposition modeling ABS. *Rapid Prototyp. J.* **8**(4), 248–257 (2002)
9. J.F. Rodríguez, J.P. Thomas, J.E. Renaud, Design of fused-deposition ABS components for stiffness and strength. *J. Mech. Des.* **125**(3), 545–551 (2003)
10. E. Ulu, E. Korkmaz, K. Yay, O.B. Ozdoganlar, L.B. Kara, Enhancing the structural performance of additively manufactured objects through build orientation optimization. *J. Mech. Des.* **137**(11), 111410–111410-9 (2015)
11. B.H. Lee, J. Abdullah, Z.A. Khan, Optimization of rapid prototyping parameters for production of flexible ABS object. *J. Mater. Process. Technol.* **169**(1), 54–61 (2005)
12. A.K. Sood, R.K. Ohdar, S.S. Mahapatra, Parametric appraisal of mechanical property of fused deposition modelling processed parts. *Mater. Des.* **31**(1), 287–295 (2010)
13. R. Anitha, S. Arunachalam, P. Radhakrishnan, Critical parameters influencing the quality of prototypes in fused deposition modelling. *J. of Mater. Process. Technol.* **118**(1–3), 385–388 (2001)
14. M. Vaezi, C.K. Chua, Effects of layer thickness and binder saturation level parameters on 3D printing process. *Int. J. Adv. Manuf. Technol.* **53**(1), 275–284 (2011)
15. R. R. Ma, L. U. Odhner, and A. M. Dollar, A modular, open-source 3d printed underactuated hand, *Robot. Auto. (ICRA)*, IEEE Int. Conf., 2013, p. 2737-2743.
16. J. Won, K. DeLaurentis, C. Mavroidis, Rapid prototyping of robotic systems. *IEEE Int. Conf. Rob. Auto.* **4**, 3077–3082 (2000)
17. K. J. De Laurentis, F. F. Kong, and C. Mavroidis, Procedure for rapid fabrication of non-assembly mechanisms with embedded components, *ASME Int. Des. Eng. Tech. Conf. Comp. Info. Eng. Conf.*, 2002, p.1239-1245.
18. J.T. Belter, A.M. Dollar, Strengthening of 3D printed fused deposition manufactured parts using the fill compositing technique. *PLoS ONE* **10**(4), e0122915 (2015)
19. Y. Jin, J. Plott, R. Chen, J. Wensman, A. Shih, Additive manufacturing of custom orthoses and prostheses—A review. *Procedia CIRP* **36**, 199–204 (2015)
20. S. Telfer, J. Pallari, J. Munguia, K. Dalgarno, M. McGeough, J. Woodburn, Embracing additive manufacture: implications for foot and ankle orthosis design. *BMC Musc. Dis.* **13**(1), 1–9 (2012)
21. “Standard test method for tensile properties of plastics”, ASTM D638-14, ASTM International, West Conshohocken, PA, 2014.
22. “Standard test method for tensile properties of polymer matrix composite materials”, ASTM D3039/D3039M – 14, ASTM International, West Conshohocken, PA, 2014.
23. L. Li, Q. Sun, C. Bellehumeur, P. Gu, Composite modeling and analysis for fabrication of FDM prototypes with locally controlled properties. *J. Manuf. Proc.* **4**(2), 129–141 (2002)
24. A.R. Torrado Perez, D.A. Roberson, and R.B. Wicker, Fracture surface analysis of 3D-printed tensile specimens of novel ABS-based materials, *J. Fail. Anal. Preven.*, 14(3), 2014, p. 343-353.